Interfacial Passivation by Polylactic Acid in Perovskite Solar Cells

Yifang Qi^a, Jing Qu^a, Jaiden Moore^a, Kristine Gollinger^a, Narendra Shrestha^b, Yongfeng Zhao^a, Nihar Pradhan^a, Jinke Tang^b, Qilin Dai^a*

^a Department of Chemistry, Physics, and Atmospheric Sciences, Jackson State University, Jackson, MS, 39217, United States.

^b Department of Physics & Astronomy, University of Wyoming, Laramie, WY 82071 USA

* Corresponding author: Q. Dai, Email: qilin.dai@jsums.edu

Abstract

Perovskite solar cells (PSCs) have attracted a lot of attention in recent years due to their high efficiency. However, this recorded performance (25.5%) is still lower than the theoretical Shockley-Queisser limit due to the defects at the surface and interface of devices. One potential strategy is to passivate the films by polymers for the PSCs owing to the tunable properties of the polymers. Herein, we introduce polylactic acid (PLA) with CH3 and C=O functional groups to passivate the interface between the perovskite and hole-transport layers. The FTIR results display the interaction of PLA and perovskite. The hole-only devices demonstrate decreased hole defect density in the PSCs by PLA passivation. Therefore, the PCE of the PSCs increases from 19.3% to 20.6%, and the Voc enhances from 1.07 V to 1.10 V as the device is treated by PLA passivation. Furthermore, PLA passivation improves the stability of the PSCs. The PSC with PLA passivation maintains ~90% of the initial PCE value, whereas the control device only keeps ~72% for 14 days. Besides, the PCE of the PSC with PLA passivation can maintain ~73 % of the original value, but the PCE of the control device decreases to ~45 % of the initial value under 60 ± 5% RH for 450 min.

Keywords: Perovskite solar cells; Passivation; Polylactic Acid; C=O groups

1. Introduction

In recent years, organic-inorganic perovskite solar cells (PSCs) attracted great attention due to the low cost, tunable bandgap with strong light absorption, long charge diffusion, and easy solvent engineering[1–5]. Up to now, the power conversion efficiency (PCE) has reached 25.5%[6] from the first reported PCE of 9.7%[7], which is attributed to some critical improvements, including the device structure engineering, the optimization of hole and electron transport layer materials, and the improved perovskite film quality by additives and interface passivation engineering[8–10]. However, the theoretical Shockley-Queisser limit of PCE value is ~30%, which is still higher than the current PCE record [11]. The defects of the perovskite films are considered to be the key reason for the limited PCE of devices. In addition, the degradation of the PSCs begins from the surface and grain boundaries in the perovskite films due to ion migration and non-radiative recombination[12–14]. To further enhance the PCE and the stability of the PSCs, some research strategies were developed including antisolvent treatment[15,16], perovskite precursor solution engineering[17,18], and in-situ surface passivation[19,20]. The passivation treatment is considered as the effective method to increase the PCE of the PSCs[21], which can decrease the defect density and suppress the charge non-radiative recombination.

Polymer with several functional groups is considered as the promising material to modify the PSCs (such as -COOH, -SH, and -NH₂), which can reduce the defect states and enhance the stability of the devices[8,22,23]. Yang *et al.* introduced the polymer with nitrile ($C \equiv N$) in the side chain of the structure into antisolvent to further improve the perovskite films, and the PCE of the devices increases from 18.18% to 22.02%[24]. Zhao *et al.* boosted the PCE of PSCs to 23% by polymer with C=O functional group to passivate the defects in the perovskite films, because the C=O function group can react with the undercoordinated lead ions[25]. However, it is still a challenge to not only heal the trap states of the perovskite films but also improve the stability of the PSCs by the passivation of the polymer under harsh humid conditions.

It is reported that poly(methyl methacrylate) (PMMA) can improve the performance of PSCs due to the C=O groups on the side chain of the PMMA, which is explained by the passivation of Pb²⁺ ions via C=O[26]. Therefore, the C=O on the side chains of PMMA are attached to the perovskite films to passivate the defects, and the backbone is hung out of the films, which is not very stable. In addition, It seems that the alkane groups (methylene, methine, and methyl groups)

on the PMMA are optional to the cell passivation. The redundant alkane groups in PMMA may increase the interface resistance of the devices, leading to decreased charge transport in the devices. It is necessary to investigate the polymer with less redundant groups to optimize the device performance.

Herein, we introduce the PLA polymer with carboxylic groups in the main chain to improve the efficiency and enhance the stability of the PSCs. The structure of the PLA monomer is similar to PMMA. The carboxylic groups are located at the backbone of PLA compared to the side-chain position of carboxylic groups on PMMA, leading to a stable connection between the PLA and perovskite films. The monomer of PLA (C₃O₂H₄) shows C₂H₄ less than PMMA (C₅O₂H₄). Therefore, the passivation effect of PLA is very promising and better than that of the PMMA. The C=O functional groups in the PLA can interact with the perovskite, which decreases the trap states and further enhances the performance of the PSCs. The PSCs modified with PLA show the PCE of 20.6% with Jsc of 24.7 mA/cm², Voc of 1.10 V, and FF of 75.8%, whereas the control device exhibits the PCE of 19.3% with Jsc of 24.6 mA/cm², Voc of 1.07 V and FF of 72.9 %. Besides, the hysteresis behavior is suppressed by the PLA passivation. Therefore, PLA passivation reduces the charge non-radiative recombination in the devices. Furthermore, the PLA passivation protects the perovskite layer from moisture, which is attributed to the long alkyl chain of polymer structure. The PSC with PLA passivation can maintain ~90% of the initial PCE, whereas the control device degrades to \sim 72% of the original value after 14 days in the condition of 25± 5%. Under 60 ± 5% RH for 450 min, the device with PLA passivation can keep ~73% of the initial PCE value and the control device decreases to ~45% of the original PCE.

2. Materials and Experiments

2.1Materials

PLA and formamidine iodide (FAI, 99%), cesium iodide (CsI, 98%), methylammonium bromide (MABr, 99.9%), chlorobenzene (CB, 99.8% anhydrous), isopropyl alcohol (IPA) and 2,2',7,7'-Tetrakis[N,N-di(4-methoxyphenyl)amino]-9,9'-spirobifluorene (Spiro-OMeTAD) were obtained from Sigma Aldrich (America). Lithium bi(trifluoromethane) sulfonimide (Li-TFSI) was received from TCI (Japan). Lead iodide (PbI₂, 99%), titanium (IV) chloride (TiCl₄, 99.9%), dimethyl sulfoxide (DMSO, 99.8 % anhydrous) and gold (Au, wires) were purchased from Alfa

Aesar (America). Lead (II) bromide (PbBr₂, 99%) was obtained from Chemsavers. 4-tert-butylpyridine(4-tBP) was purchased from Accela (America). Patterned fluorine doped tin oxide glass substrates were purchased from Advanced Election Technology Co., Ltd (China).

2.2 Device Fabrication

The FTO-coated glasses are used as substrates in this work. The substrates were cleaned sequentially with detergent, acetone, deionized water, and isopropanol with ultrasonic cleaning for 15 min. After that, the substrates were dried by N₂ flowing and then were treated with ultravioletozone to remove the remaining organic solvent on the films for 30 min. For this work, the electron transport layer TiO₂ was synthesized by the sol-gel method. TiCl₄ was diluted in 150 mL deionized water at 0 °C to obtain TiCl₄ solution (0.2 M), and then the FTO substrates were put into the TiCl₄ solution to fabricate the TiO2 layer in a water bath at 60 °C for 60 min. Next, the substrates were washed with deionized water and isopropanol for 5 min, and then the substrates were annealed at 200 °C for 30 min to form FTO/ TiO₂ films. Then the films were transferred to the glove box to prepare the perovskite layer. PbI₂ (1.1 M), PbBr₂ (0.2 M), MABr (0.2 M), and FAI (1 M) were dissolved in the mixed solvents (DMF: DMSO=4:1, volume ratio) to obtain the perovskite precursor solution. Then 40 µl CsI solution (1.5 M in 1 mL DMSO) was dropped into the perovskite precursor solution. The perovskite precursor solution was spin-coated on TiO₂ layer with 2000 rpm for 40 s, and chlorobenzene as anti-solvent was dropped on the spinning substrates with 4000 rpm at the last 20 s, and then the films were annealed 60 min to form Cs_{0.05}(FA_{0.83}MA_{0.17})_{0.95}Pb(I_{0.83}Br_{0.17})₃ perovskite films. After that, the PLA solutions with different concentrations in chloroform were spin-coated onto the perovskite films and annealed for 10 min under 70 °C. For the hole transport layer, 72.3 mg of Spiro-OMeTAD was dissolved in 1 mL chlorobenzene with adding 28.8 µL of 4-tertbutylpyridine and 17.5 µL of bis (trifluoromethylsulfonyl) imide lithium solution (520 mg in 1 mL acetonitrile). The Sprio-OMeTAD solution was spin-coated on the perovskite layer at 4000 rpm for 30 s. Finally, the gold (Au) electrode was thermal evaporated on the top of the Spiro-MeOTAD layer after oxidation for 12 h. The device area is 0.1 cm² decided by the shadow masks.

2.3 Film Characterization

The perovskite film surface morphology information was studied by scanning electron microscopy (SEM) with a field emission scanning electron microscope (LYR3 XMH, Tescan) and atomic force microscopy (AFM) (Bruker Dimension Icon Scanning Probe Microscope). The UV-vis absorption spectra were obtained by Cary 60 UV-vis spectrophotometer (Agilent Technologies). The current-voltage (JV) curves were measured by a digital source meter (Keithley, 2400, USA) under the illumination AM1.5G (100 mW/cm²). The steady-state photoluminescence (PL) spectra and the time-resolved photoluminescence (TRPL) were collected by the fluorescence spectrometer (FluoroMax, Horiba) with DeltaHub and NanoLED. The electrochemical impedance spectroscopy (EIS) of the PSCs was measured by the electrochemical workstation (CHI 604E) to investigate the series and non-radiative recombination resistances of the PSCs. For the EIS measurement, the PSCs were swept from 1 Hz to 1 M Hz frequency with 0.9 bias in the dark. The monochromatic external quantum efficiency (EQE) was obtained by the quantum efficiency measurement system (IQE-200B, Newport). In addition, the JV curves of the hole-only devices were measured by source meter (Keithley, 2450, USA). The crystallization of perovskite film was studied by XRD with a Rigaku Smart Lab X-ray Diffractometer from 10 degrees to 40 degrees.

3. Results and discussions

Figure 1a shows the fourier infrared transmittance (FTIR) spectra of perovskite films with and without PLA passivation, in which the C-O binding peak exhibits redshift from 3266 cm⁻¹ to 3261 cm⁻¹ as the perovskite film is modified by PLA. The redshift indicates the interaction between PLA and perovskite films. Figure S1 exhibits the FTIR spectra of PLA, perovskite film, and perovskite film with PLA passivation. The FTIR spectrum of PLA shows the peaks of 1750 cm⁻¹, 1454 cm⁻¹, and 1284 cm⁻¹, which are attributed to functional groups of C=O, C-H, and C-O respectively [27,28]. Very tiny peaks at similar positions are also observed in perovskite film with PLA passivation, but the peak intensities are very weak, indicating a limited amount of PLA is in the perovskite films (Figure 1a), since the perovskite films are scratched out from the substrates to obtain the corresponding powder for the FTIR measurement, leading to the PLA on the film surface is mixed into the perovskite powder. Figure 1b displays the crystallization of perovskite films with and without PLA passivation. The peaks at 14.1°, 20.0°, 24.5°, 28.3°, 31.8°, and 34.9° are attributed to (100), (110), (111), (200), (210), and (211) crystal planes. The perovskite films with and without passivation look identical in terms of peak positions. Therefore, the crystal structure is not

influenced by passivation. The structure of the PSCs is shown in Figure 1c (FTO/TiO₂/perovskite with PLA/Spiro-OMeTAD /Au). TiO₂ is employed as the electron transport layer, and Spiro-OMeTAD is used as the hole transport layer. PLA is used to modify the perovskite films and the molecule structure is illustrated in Figure 1d. The PLA passivation mechanism is illustrated in Figure 1d. The PLA shows significant potential to passivate the defects in the perovskite films and improve the carrier extraction due to the C=O functional groups in the PLA structure[29].

To study the PLA influence on the morphology and flatness of perovskite films, SEM and AFM measurements are carried out. Figures 2a and b exhibit the top-view SEM images of perovskite films without and with PLA passivation. Two compact and uniform films show very similar grain sizes (~250 nm). PLA passivation has no negative effects on the surface morphology. In addition, Figures 2c and d show the cross-section SEM images of perovskite films without and with

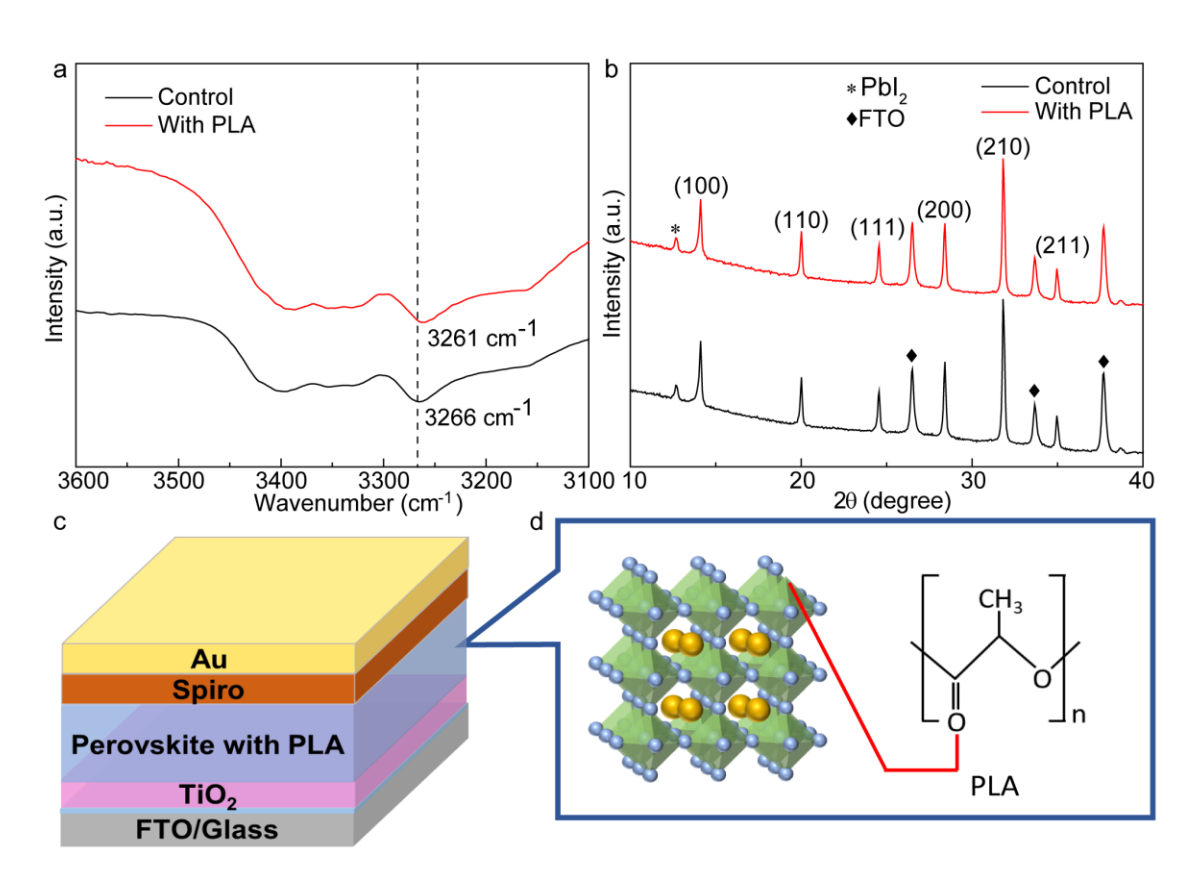


Figure 1. a The FTIR spectra of perovskite films with and without PLA; b The XRD diffraction patterns of perovskite films with and without PLA; c The device structure of the modified PSCs; d PLA passivation principle on perovskite.

passivation, which indicate the thickness of ~550 nm for the two perovskite films. The surface

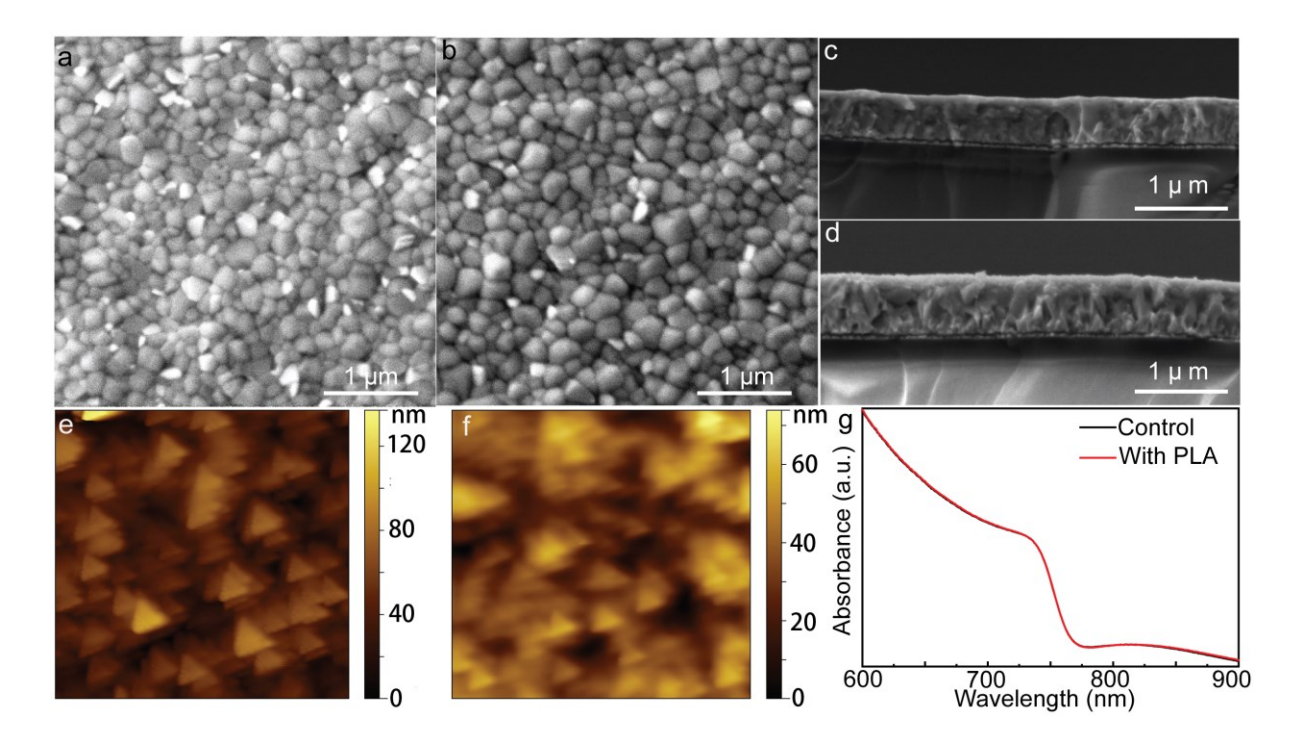


Figure 2. a-b The top-view SEM images of perovskite films without and with PLA; c-d The cross-section SEM images of PSCs without and with PLA; e-f The AFM images of perovskite films without and with PLA; g The UV-vis absorption spectra of perovskite films with and without PLA.

roughness results of perovskite films without and with PLA modification are obtained by AFM measurements, as illustrated in Figure 2e and f. The root-mean-square roughness (RMS) of perovskite film decreases from 66 nm to 45 nm after passivation by PLA. Thus, the PLA passivation smoothes the perovskite film, which can improve the carrier extraction and transport in the PSCs. Figure 2g displays the UV-vis absorption spectra of perovskite films with and without PLA passivation, which shows the perovskite peaks at ~740 nm. In addition, the perovskite film with PLA passivation exhibits the same peak, indicating the PLA passivation does not influence the light-harvesting of the perovskite layer. We measure the transmittance spectra of FTO conductive glass coated with different PLA concentrations (2 mg/mL, 1 mg/mL, 0.5 mg/mL, and 0 mg/mL). The PLA has little influence on the transmittance of conductive glass (Figure S2). However, the PLA passivation layer is on top of the perovskite layer, and the incident light is irradiated from the FTO side. Hence, the PLA passivation layer cannot affect the light absorption of the device due to the device structure of FTO/TiO₂/perovskite with PLA/Spiro/ Au.

We further study the influence of PLA passivation on PSC performance. Figure S3 shows the photovoltaic parameters of the devices with different PLA concentrations. It can be seen that the optimized PLA concentration is 1 mg/mL. Figures 3a and b illustrate the Voc and PCE of PSCs without and with PLA passivation (1 mg/mL). The average Voc of PSCs increases from ~1.07 V to ~1.10 V, and the average PCE of devices increases from ~18.5% to 19.5% as the devices are modified by the PLA, which is attributed to the trap state modification of the PSCs after PLA passivation[30,31]. In addition, Figure 3c displays the J-V curves of the champion PSCs with and without PLA passivation. The champion PSC with PLA passivation shows a PCE of 20.6% with Jsc of 24.7 mA/cm², Voc of 1.10 V, and FF of 75.8%, whereas the control device exhibits the PCE of 19.3% with Jsc of 24.6 mA/cm², Voc of 1.07 V and FF of 72.9 %. The PLA passivation decreases the defect density and further improves the performance of the PSCs by the interaction between PLA and perovskite films. Furthermore, Figure 3d displays the J-V curves of the PSCs with and without PLA passivation under forward and reverse scan directions. The hysteresis index values are calculated by the following equation:

$$HI = \frac{PCE_{reversed} - PCE_{forward}}{PCE_{reversed}}$$

where PCE_{reversed} is the device PCE obtained by reverse scan direction, and PCE_{forward} is the PCE of the device with forward scan direction. The PCE of the control device under reverse scan direction is 18.53 %, and 17.40 % is obtained with the forward scan direction. However, the PCE values of the device with PLA passivation are 19.88 % and 19.49 % for reverse and forward directions, respectively. The calculated HI values of the devices with and without PLA passivation are 0.019 and 0.061, respectively. It is obvious to see that the PLA passivation reduces the hysteresis behavior of the PSCs. PLA passivation decreases the defect density and suppresses the charge recombination at the interface of the perovskite layer and spiro-OMeTAD[32–34]. Figure 3e shows photocurrent density and PCE stability of devices with and without PLA under continuous light irradiation for 180 s. It can be observed that the modified device shows better stability than the control device.

Steady-state photoluminescence (PL) and time-resolved PL (TRPL) measurements of perovskite films on FTO are carried out to study the influence of PLA passivation on charge extraction and lifetime, as shown in Figures 4a and b. Compared to the control sample, the PL

spectrum of the perovskite film with PLA passivation exhibits a higher intensity, which indicates

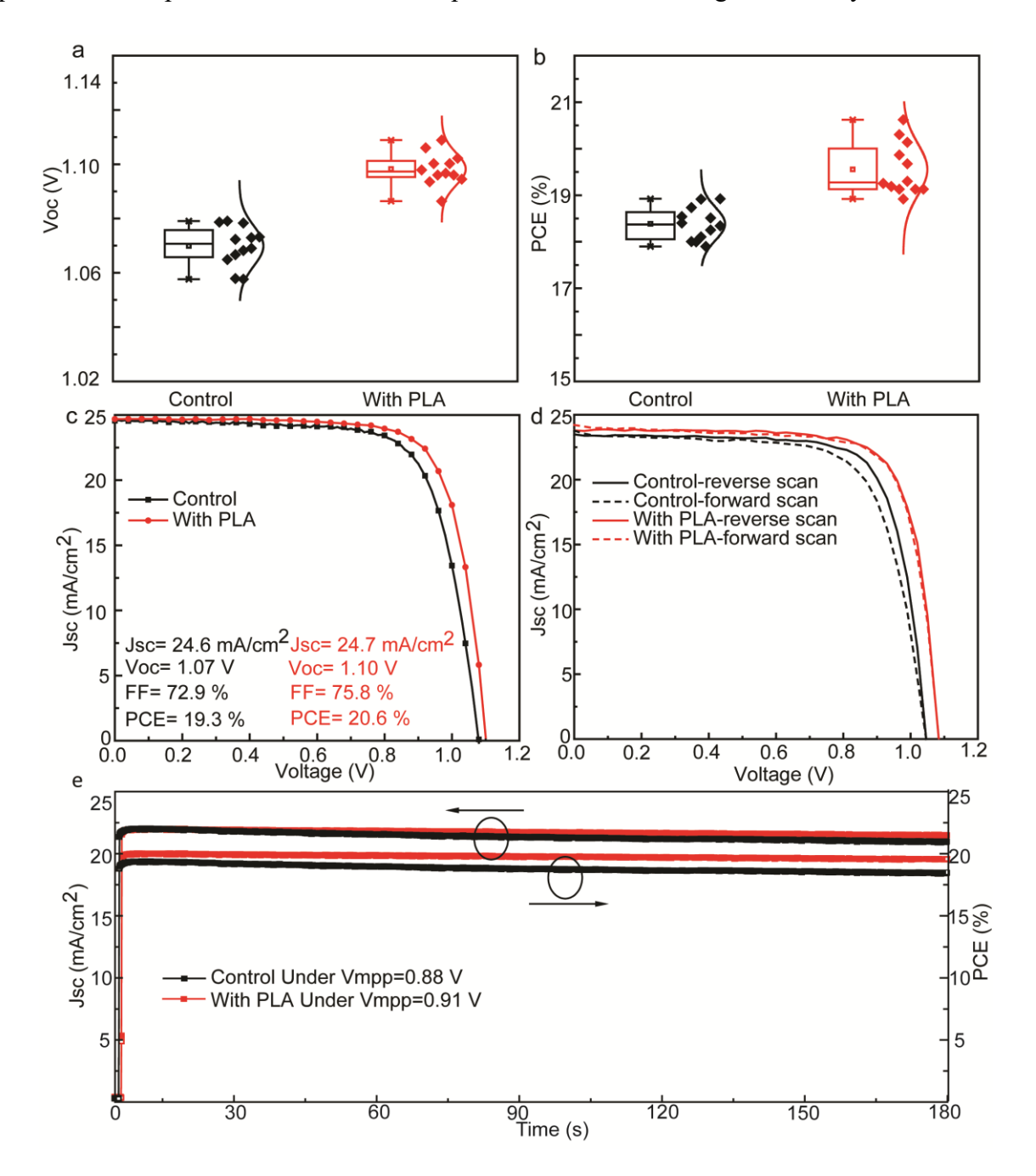


Figure 3. a-b The histograms of Voc and PCE values of PSCs with and without PLA; c The J-V curves of champion devices with and without PLA; d The J-V curves of PSCs with PLA under different scan directions. e The steady-state current density and PCE output of the PSCs with and without PLA.

the PLA passivation suppresses the carrier non-radiative recombination of perovskite films[35–37]. Besides, the TRPL spectra in Figure 4b are fitted by the biexponential decay equation:

$$Y = A_1 \exp\left(\frac{-t}{\tau_1}\right) + A_2 \exp\left(\frac{-t}{\tau_2}\right)$$

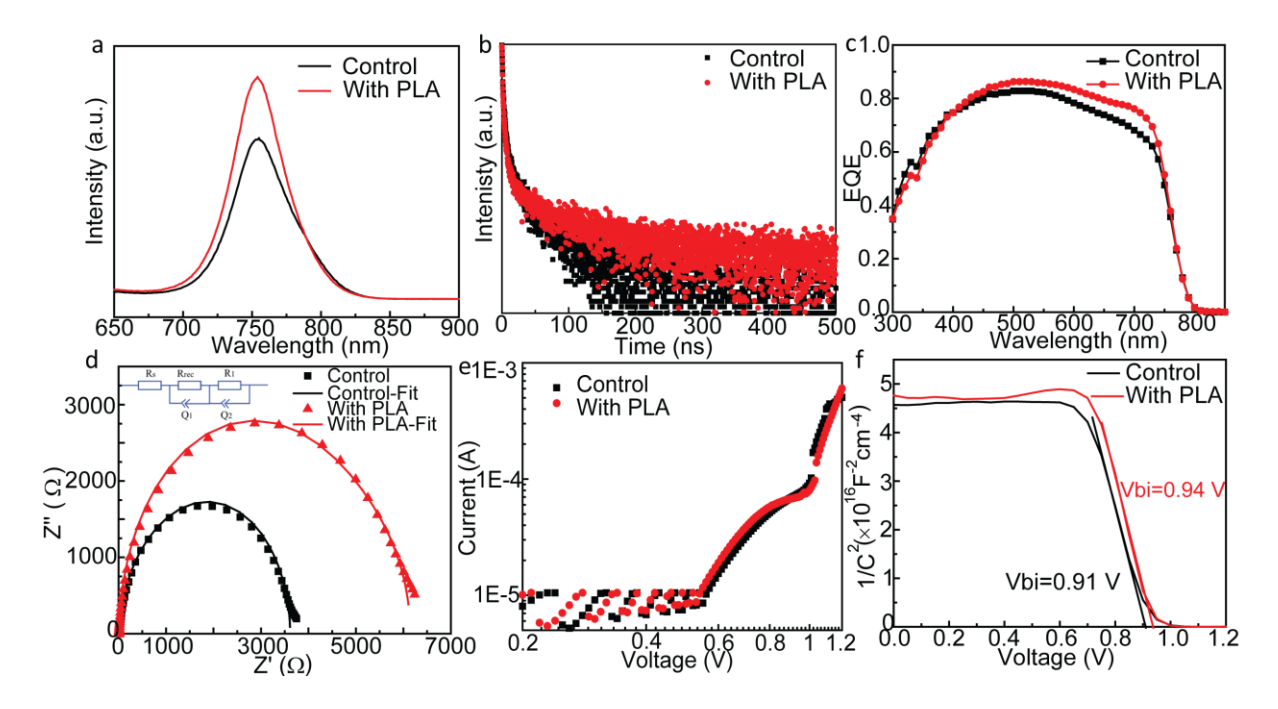


Figure 4. a-b The PL and TRPL spectra of perovskite films with and without PLA; c The EQE of PSCs with and without PLA; d The Nyquist plot of the PSCs with and without PLA; e The JV curves of hole-only devices with and without PLA; f The Mott-Schottky measurements for PSCs with and without PLA.

where τ_1 and τ_2 stand for fast and slow decay time constants, respectively. The fast decay (τ_1) is attributed to carriers trapping in the defects in the perovskite films, and the slow decay (τ_2) is assigned to the charge radiative recombination[38,39]. The fitted τ_1 and τ_2 values of the control perovskite film are 47 ns and 191 ns, whereas the τ_1 and τ_2 values for perovskite film with PLA passivation are 82 and 330 ns. Thus, the PLA passivation enhances the lifetime of perovskite films and further improves the performance of devices. The external quantum efficiency (EQE) spectra of the perovskite films with and without passivation are displayed in Figure 4c, which exhibit the photo-response ranging from 300 nm to 850 nm in the PSCs with and without PLA passivation. Compared to the control device, the EQE spectrum of the device with PLA passivation shows a little higher photo-response, which is attributed to the increased carrier extract and transport at the interface due to PLA passivation[40,41]. Electrochemical impedance spectroscopy (EIS) measurements are performed to investigate the charge transport processes in the PSCs with and

without PLA passivation, as illustrated in Figure 4d. Besides, the fitting circuit is shown in the inset of Figure 4d. In the Nyquist plot, series resistance (Rs) decreases from 32.5 Ω to 18.1 Ω , and the recombination resistance Rrec increases from 2044 Ω to 5399 Ω due to PLA passivation, indicating PLA passivation facilitates charge transport and further enhances FF of the PSCs[42]. To further investigate the PLA passivation influence on the defect density of the interface between perovskite and Spiro-OMeTAD layer, we fabricate the hole-only devices with and without PLA passivation (Figure 4e), and the structure of hole-only devices is FTO/PTAA/perovskite with and without PLA/Spiro-OMeTAD/Au. There are three behaviors in the J-V curves of hole-only devices, including an ohmic region (n=1), a trap-filled limit (TFL) region (n>3), and a space-charge limited current (SCLC) region (n=2)[43,44]. The hole defect density in the PSCs can be calculated by the equation:

$$V_{TFL} = \frac{en_t L^2}{2\varepsilon\varepsilon_0}$$

where n_t is the defect density in the perovskite films; V_{TFL} is the onset voltage in the TFL region; L is the perovskite film thickness; e is the elementary charge of an electron; ϵ stand for the relative dielectric constant of MAPbI₃ and ϵ_0 is the vacuum dielectric constant. The calculated hole defect density of the control device is 3.17×10^{18} cm⁻³, whereas the hole defect density for the PSCs with PLA passivation is 3×10^{18} cm⁻³. The PLA passivation reduces the hole defect density at the interface of the perovskite film/Spiro-OMeTAD in the PSCs. Figure S4 shows the electron-only devices with the structure of TiO₂/perovskite/PC₆₁BM/Ag. The electron trap densities of PSCs

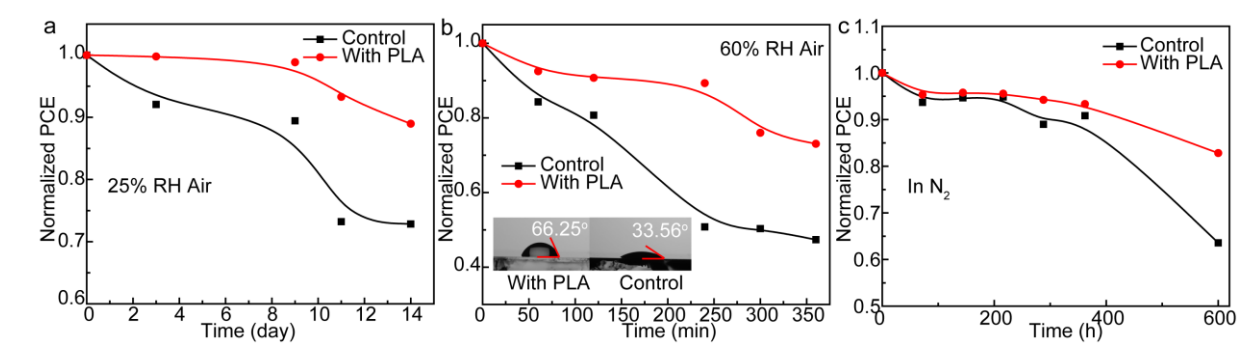


Figure 5. a The stability of PSCs with and without PLA in an ambient environment with RH condition of $25 \pm 5\%$; b The stability of PSCs and water contact angles of perovskite films with and without PLA in an ambient environment with an RH condition of $60 \pm 5\%$; c The stability of PSCs with and without PLA in N₂ environment.

without and with PLA are estimated to be 2.93×10¹⁶ cm⁻³ and 2.20×10¹⁶ cm⁻³, respectively.

Therefore, the PLA passivation decreases the electron and hole trap densities. Figure 4f exhibits the $1/C^2$ plots of PSCs with and without PLA passivation which are obtained by the capacitance-voltage (C–V) measurement. As shown in Figure 4f, the V_{bi} values of the devices with and without PLA passivation are 0.94 V and 0.91V, and this result is consistent with the increased Voc of the PSCs from 1.07 V to 1.10 V (Figure 2a). Thus, PLA passivation improves the charge diffusion and injection of the devices[45].

In addition, we study the long-term and moisture stability of the devices with and without PLA passivation. The stability of the devices under $25 \pm 5\%$ relative humidity (RH) and $30 \pm 5\%$ conditions for 14 days is shown in Figure 5a. The control device degrades to ~72% of the initial PCE, whereas the PSC with PLA passivation can keep ~90% of the original value for 14 days. Furthermore, the PCE of the PSC with PLA passivation can maintain ~73 % of the original values, but the PCE of the control device decreases to \sim 45 % of the initial values under 60 \pm 5% RH for 360 min, as illustrated in Figure 5b. Besides, the water contact angles of the perovskite films with and without PLA are shown in the inset of Figure 5b. The water contact angle values for the perovskite with PLA and control films are 66.25° and 33.56° respectively, which can explain the improved stability of the devices under high humidity condonation because the perovskite film is much hydrophobic after passivation of PLA. Figure 5c exhibits the stability of PSCs with and without PLA in N₂ environment. The device with PLA keeps 83% of the initial PCE value, but the control device only could maintain 64% of its initial value after 600 h, which suggests the PLA passivation suppresses the ion migration in the interface and then enhance the stability of PSCs. Therefore, the PLA passivation protects the PSCs from moisture corrosion and further enhances the stability of devices, which is attributed to the decreased defects and reduced ion migration in the devices caused by PLA.

4. Conclusions

In summary, we demonstrate an effective interface engineering strategy, where polymer molecules containing C=O and CH₃ functional groups are introduced to modify the interface between perovskite and hole-transport layers. The PLA passivation can suppress the carrier non-radiative recombination and decrease the trap states at the interface by interacting with the uncoordinated Pb²⁺, which is confirmed by the PL, TRPL, and EIS results. The PSCs with PLA passivation exhibit the PCE of 20.60% and the average Voc of the devices increases from 1.07 V

to 1.10V. Furthermore, PLA passivation can protect the PSCs from moisture and decreases the degradation rate of the devices. The PSC with PLA passivation maintains \sim 90% of the initial PCE values, whereas the control device keeps \sim 72% for 14 days in the condition of under 25 \pm 5% RH. Besides, the PCE of the PSC with PLA passivation can maintain \sim 73 % of the original value, but the PCE of the control device decreases to \sim 45 % of the initial values under 60 \pm 5% RH for 360 min.

Acknowledgment

This material is based on work supported by the National Science Foundation under Grant No. 1757220. The steady-state PL and TRPL equipment used in this work is supported by National Science Foundation Research Initiation Award: Novel Perovskite Solar Cells Based on Interface Manipulation (Award#1900047).

Reference

- [1] J.J. Yoo, G. Seo, M.R. Chua, T.G. Park, Y. Lu, F. Rotermund, Y.-K. Kim, C.S. Moon, N.J. Jeon, J.-P. Correa-Baena, V. Bulović, S.S. Shin, M.G. Bawendi, J. Seo, Efficient perovskite solar cells via improved carrier management, Nature. 590 (2021) 587–593. https://doi.org/10.1038/s41586-021-03285-w.
- [2] J. Mingyu, C.I. Woo, G.E. Min, C. Yongjoon, K. Minjin, L. Byongkyu, J. Seonghun, J. Yimhyun, C.H. Won, L. Jiyun, B. Jin-Hyuk, K.S. Kyu, K.D. Suk, Y. Changduk, Stable perovskite solar cells with efficiency exceeding 24.8% and 0.3-V voltage loss, Science (80-.). 369 (2020) 1615–1620. https://doi.org/10.1126/science.abb7167.
- [3] J. Ali, Y. Li, P. Gao, T. Hao, J. Song, Q. Zhang, L. Zhu, J. Wang, W. Feng, H. Hu, F. Liu, Interfacial and structural modifications in perovskite solar cells, Nanoscale. 12 (2020) 5719–5745. https://doi.org/10.1039/c9nr10788f.
- [4] E.H. Jung, N.J. Jeon, E.Y. Park, C.S. Moon, T.J. Shin, T.-Y. Yang, J.H. Noh, J. Seo, Efficient, stable and scalable perovskite solar cells using poly(3-hexylthiophene), Nature.

- 567 (2019) 511–515. https://doi.org/10.1038/s41586-019-1036-3.
- [5] J.J. Yoo, S. Wieghold, M.C. Sponseller, M.R. Chua, S.N. Bertram, N.T.P. Hartono, J.S. Tresback, E.C. Hansen, J.-P. Correa-Baena, V. Bulović, T. Buonassisi, S.S. Shin, M.G. Bawendi, An interface stabilized perovskite solar cell with high stabilized efficiency and low voltage loss, Energy Environ. Sci. 12 (2019) 2192–2199. https://doi.org/10.1039/c9ee00751b.
- [6] NREL, Best-Research-Cell-Efficiencies-Rev210726.Pdf, (n.d.).
- [7] H.-S. Kim, C.-R. Lee, J.-H. Im, K.-B. Lee, T. Moehl, A. Marchioro, S.-J. Moon, R. Humphry-Baker, J.-H. Yum, J.E. Moser, M. Grätzel, N.-G. Park, Lead Iodide Perovskite Sensitized All-Solid-State Submicron Thin Film Mesoscopic Solar Cell with Efficiency Exceeding 9%, Sci. Rep. 2 (2012). https://doi.org/10.1038/srep00591.
- [8] J. Zheng, J. Chen, D. Ouyang, Z. Huang, X. He, J. Kim, W.C.H. Choy, Critical Role of Functional Groups in Defect Passivation and Energy Band Modulation in Efficient and Stable Inverted Perovskite Solar Cells Exceeding 21% Efficiency, ACS Appl. Mater. Interfaces. 12 (2020) 57165–57173. https://doi.org/10.1021/acsami.0c18862.
- [9] X. Ren, Z. Wang, W.E.I. Sha, W.C.H. Choy, Exploring the Way To Approach the Efficiency Limit of Perovskite Solar Cells by Drift-Diffusion Model, ACS Photonics. 4 (2017) 934–942. https://doi.org/10.1021/acsphotonics.6b01043.
- [10] W.E.I. Sha, X. Ren, L. Chen, W.C.H. Choy, The efficiency limit of CH3NH3PbI3 perovskite solar cells, Appl. Phys. Lett. 106 (2015) 221104. https://doi.org/10.1063/1.4922150.
- [11] M. Stolterfoht, C.M. Wolff, Y. Amir, A. Paulke, L. Perdigón-Toro, P. Caprioglio, D. Neher, Approaching the fill factor Shockley–Queisser limit in stable, dopant-free triple cation perovskite solar cells, Energy Environ. Sci. 10 (2017) 1530–1539. https://doi.org/10.1039/c7ee00899f.
- [12] J. Luo, J. Xia, H. Yang, C. Sun, N. Li, H.A. Malik, H. Shu, Z. Wan, H. Zhang, C.J. Brabec, C. Jia, A pressure process for efficient and stable perovskite solar cells, Nano Energy. 77 (2020) 105063. https://doi.org/10.1016/j.nanoen.2020.105063.

- [13] R.K. Gupta, R. Garai, M. Hossain, A. Choudhury, P.K. Iyer, Halide Engineering for Mitigating Ion Migration and Defect States in Hot-Cast Perovskite Solar Cells, ACS Sustain. Chem. Eng. 9 (2021) 7993–8001. https://doi.org/10.1021/acssuschemeng.1c02537.
- [14] S. Tan, I. Yavuz, N. De Marco, T. Huang, S. Lee, C.S. Choi, M. Wang, S. Nuryyeva, R. Wang, Y. Zhao, H. Wang, T. Han, B. Dunn, Y. Huang, J. Lee, Y. Yang, Steric Impediment of Ion Migration Contributes to Improved Operational Stability of Perovskite Solar Cells, Adv. Mater. 32 (2020) 1906995. https://doi.org/10.1002/adma.201906995.
- [15] S. Ghosh, S. Mishra, T. Singh, Antisolvents in Perovskite Solar Cells: Importance, Issues, and Alternatives, Adv. Mater. Interfaces. 7 (2020) 2000950. https://doi.org/10.1002/admi.202000950.
- [16] M. Li, X. Yan, Z. Kang, X. Liao, Y. Li, X. Zheng, P. Lin, J. Meng, Y. Zhang, Enhanced Efficiency and Stability of Perovskite Solar Cells via Anti-Solvent Treatment in Two-Step Deposition Method, ACS Appl. Mater. Interfaces. 9 (2017) 7224–7231. https://doi.org/10.1021/acsami.7b01136.
- [17] S. Tang, Y. Deng, X. Zheng, Y. Bai, Y. Fang, Q. Dong, H. Wei, J. Huang, Composition Engineering in Doctor-Blading of Perovskite Solar Cells, Adv. Energy Mater. 7 (2017) 1700302. https://doi.org/10.1002/aenm.201700302.
- [18] X. Wu, Y. Jiang, C. Chen, J. Guo, X. Kong, Y. Feng, S. Wu, X. Gao, X. Lu, Q. Wang, G. Zhou, Y. Chen, J. Liu, K. Kempa, J. Gao, Stable Triple Cation Perovskite Precursor for Highly Efficient Perovskite Solar Cells Enabled by Interaction with 18C6 Stabilizer, Adv. Funct. Mater. 30 (2019) 1908613. https://doi.org/10.1002/adfm.201908613.
- [19] M.A. Mahmud, T. Duong, Y. Yin, J. Peng, Y. Wu, T. Lu, H.T. Pham, H. Shen, D. Walter, H.T. Nguyen, N. Mozaffari, G.D. Tabi, Y. Liu, G. Andersson, K.R. Catchpole, K.J. Weber, T.P. White, In Situ Formation of Mixed-Dimensional Surface Passivation Layers in Perovskite Solar Cells with Dual-Isomer Alkylammonium Cations, Small. 16 (2020) 2005022. https://doi.org/10.1002/smll.202005022.
- [20] F. Tan, H. Tan, M.I. Saidaminov, M. Wei, M. Liu, A. Mei, P. Li, B. Zhang, C. Tan, X. Gong, Y. Zhao, A.R. Kirmani, Z. Huang, J.Z. Fan, R. Quintero-Bermudez, J. Kim, Y. Zhao, O.

- Voznyy, Y. Gao, F. Zhang, L.J. Richter, Z. Lu, W. Zhang, E.H. Sargent, In Situ Back-Contact Passivation Improves Photovoltage and Fill Factor in Perovskite Solar Cells, Adv. Mater. 31 (2019) 1807435. https://doi.org/10.1002/adma.201807435.
- [21] Y. Xu, G. Li, R. Li, Y. Jing, H. Zhang, X. Wang, Z. Du, J. Wu, Z. Lan, PbS/CdS heterojunction thin layer affords high-performance carbon-based all-inorganic solar cells, Nano Energy. 95 (2022) 106973. https://doi.org/10.1016/j.nanoen.2022.106973.
- [22] T. Li, S. Wang, J. Yang, X. Pu, B. Gao, Z. He, Q. Cao, J. Han, X. Li, Multiple functional groups synergistically improve the performance of inverted planar perovskite solar cells, Nano Energy. 82 (2021) 105742. https://doi.org/10.1016/j.nanoen.2021.105742.
- [23] L. Xie, J. Chen, P. Vashishtha, X. Zhao, G.S. Shin, S.G. Mhaisalkar, N.-G. Park, Importance of Functional Groups in Cross-Linking Methoxysilane Additives for High-Efficiency and Stable Perovskite Solar Cells, ACS Energy Lett. 4 (2019) 2192–2200. https://doi.org/10.1021/acsenergylett.9b01356.
- [24] J. Yang, Q. Cao, Z. He, X. Pu, T. Li, B. Gao, X. Li, The poly(styrene-co-acrylonitrile) polymer assisted preparation of high-performance inverted perovskite solar cells with efficiency exceeding 22%, Nano Energy. 82 (2021) 105731. https://doi.org/10.1016/j.nanoen.2020.105731.
- [25] Y. Zhao, P. Zhu, M. Wang, S. Huang, Z. Zhao, S. Tan, T. Han, J. Lee, T. Huang, R. Wang, J. Xue, D. Meng, Y. Huang, J. Marian, J. Zhu, Y. Yang, A Polymerization-Assisted Grain Growth Strategy for Efficient and Stable Perovskite Solar Cells, Adv. Mater. 32 (2020) 1907769. https://doi.org/10.1002/adma.201907769.
- [26] J. Peng, J.I. Khan, W. Liu, E. Ugur, T. Duong, Y. Wu, H. Shen, K. Wang, H. Dang, E. Aydin, X. Yang, Y. Wan, K.J. Weber, K.R. Catchpole, F. Laquai, S. Wolf, T.P. White, A Universal Double-Side Passivation for High Open-Circuit Voltage in Perovskite Solar Cells: Role of Carbonyl Groups in Poly(methyl methacrylate), Adv. Energy Mater. 8 (2018) 1801208. https://doi.org/10.1002/aenm.201801208.
- [27] M.A. Cuiffo, J. Snyder, A.M. Elliott, N. Romero, S. Kannan, G.P. Halada, Impact of the Fused Deposition (FDM) Printing Process on Polylactic Acid (PLA) Chemistry and

- Structure, Appl. Sci. . 7 (2017). https://doi.org/10.3390/app7060579.
- [28] B.W. Chieng, N.A. Ibrahim, W.M. Yunus, M.Z. Hussein, Poly(lactic acid)/Poly(ethylene glycol) Polymer Nanocomposites: Effects of Graphene Nanoplatelets, Polym. . 6 (2014). https://doi.org/10.3390/polym6010093.
- [29] W. Rui, X. Jingjing, W. Kai-Li, W. Zhao-Kui, L. Yanqi, F. David, X. Guangwei, N. Selbi, H. Tianyi, Z. Yepin, Y.J. Lee, Z. Jiahui, W. Minhuan, T. Shaun, Y. Ilhan, H.K. N., Y. Yang, Constructive molecular configurations for surface-defect passivation of perovskite photovoltaics, Science (80-.). 366 (2019) 1509–1513. https://doi.org/10.1126/science.aay9698.
- [30] X. Zhou, L. Zhang, X. Wang, C. Liu, S. Chen, M. Zhang, X. Li, W. Yi, B. Xu, Highly Efficient and Stable GABr-Modified Ideal-Bandgap (1.35 eV) Sn/Pb Perovskite Solar Cells Achieve 20.63% Efficiency with a Record Small V oc Deficit of 0.33 V, Adv. Mater. 32 (2020) 1908107. https://doi.org/10.1002/adma.201908107.
- [31] Q. Zhou, Q. Xiong, Z. Zhang, J. Hu, F. Lin, L. Liang, T. Wu, X. Wang, J. Wu, B. Zhang, P. Gao, Fluoroaromatic Cation-Assisted Planar Junction Perovskite Solar Cells with Improved V OC and Stability: The Role of Fluorination Position, Sol. RRL. 4 (2020) 2000107. https://doi.org/10.1002/solr.202000107.
- [32] T. Bu, J. Li, W. Huang, W. Mao, F. Zheng, P. Bi, X. Hao, J. Zhong, Y.-B. Cheng, F. Huang, Surface modification via self-assembling large cations for improved performance and modulated hysteresis of perovskite solar cells, J. Mater. Chem. A. 7 (2019) 6793–6800. https://doi.org/10.1039/c8ta12284a.
- [33] S.-H. Turren-Cruz, M. Saliba, M.T. Mayer, H. Juárez-Santiesteban, X. Mathew, L. Nienhaus, W. Tress, M.P. Erodici, M.-J. Sher, M.G. Bawendi, M. Grätzel, A. Abate, A. Hagfeldt, J.-P. Correa-Baena, Enhanced charge carrier mobility and lifetime suppress hysteresis and improve efficiency in planar perovskite solar cells, Energy Environ. Sci. 11 (2018) 78–86. https://doi.org/10.1039/c7ee02901b.
- [34] H. Yoon, S.M. Kang, J.-K. Lee, M. Choi, Hysteresis-free low-temperature-processed planar perovskite solar cells with 19.1% efficiency, Energy Environ. Sci. 9 (2016) 2262–2266.

- https://doi.org/10.1039/c6ee01037g.
- [35] M. Kim, G.-H. Kim, T.K. Lee, I.W. Choi, H.W. Choi, Y. Jo, Y.J. Yoon, J.W. Kim, J. Lee, D. Huh, H. Lee, S.K. Kwak, J.Y. Kim, D.S. Kim, Methylammonium Chloride Induces Intermediate Phase Stabilization for Efficient Perovskite Solar Cells, Joule. 3 (2019) 2179–2192. https://doi.org/10.1016/j.joule.2019.06.014.
- [36] T. Du, W. Xu, M. Daboczi, J. Kim, S. Xu, C.-T. Lin, H. Kang, K. Lee, M.J. Heeney, J.-S. Kim, J.R. Durrant, M.A. McLachlan, p-Doping of organic hole transport layers in p-i-n perovskite solar cells: correlating open-circuit voltage and photoluminescence quenching, J. Mater. Chem. A. 7 (2019) 18971–18979. https://doi.org/10.1039/c9ta03896e.
- [37] W. Chen, Y. Zhou, G. Chen, Y. Wu, B. Tu, F. Liu, L. Huang, A.M.C. Ng, A.B. Djurišić, Z. He, Alkali Chlorides for the Suppression of the Interfacial Recombination in Inverted Planar Perovskite Solar Cells, Adv. Energy Mater. 9 (2019) 1803872. https://doi.org/10.1002/aenm.201803872.
- [38] D.-H. Kang, N.-G. Park, On the Current–Voltage Hysteresis in Perovskite Solar Cells: Dependence on Perovskite Composition and Methods to Remove Hysteresis, Adv. Mater. 31 (2019) 1805214. https://doi.org/https://doi.org/10.1002/adma.201805214.
- [39] C. Ma, N.-G. Park, Paradoxical Approach with a Hydrophilic Passivation Layer for Moisture-Stable, 23% Efficient Perovskite Solar Cells, ACS Energy Lett. 5 (2020) 3268– 3275. https://doi.org/10.1021/acsenergylett.0c01848.
- [40] K.M. Boopathi, R. Mohan, T.-Y. Huang, W. Budiawan, M.-Y. Lin, C.-H. Lee, K.-C. Ho, C.-W. Chu, Synergistic improvements in stability and performance of lead iodide perovskite solar cells incorporating salt additives, J. Mater. Chem. A. 4 (2016) 1591–1597. https://doi.org/10.1039/c5ta10288j.
- [41] K. Deng, Z. Liu, M. Wang, L. Li, Nanoimprinted Grating-Embedded Perovskite Solar Cells with Improved Light Management, Adv. Funct. Mater. 29 (2019) 1900830. https://doi.org/10.1002/adfm.201900830.
- [42] Y. Zhao, P. Zhu, S. Huang, S. Tan, M. Wang, R. Wang, J. Xue, T.-H. Han, S.-J. Lee, A. Zhang, T. Huang, P. Cheng, D. Meng, J.-W. Lee, J. Marian, J. Zhu, Y. Yang, Molecular

- Interaction Regulates the Performance and Longevity of Defect Passivation for Metal Halide Perovskite Solar Cells, J. Am. Chem. Soc. 142 (2020) 20071–20079. https://doi.org/10.1021/jacs.0c09560.
- [43] M. Sajedi Alvar, P.W.M. Blom, G.-J.A.H. Wetzelaer, Space-charge-limited electron and hole currents in hybrid organic-inorganic perovskites, Nat. Commun. 11 (2020). https://doi.org/10.1038/s41467-020-17868-0.
- [44] E.A. Duijnstee, J.M. Ball, V.M. Le Corre, L.J.A. Koster, H.J. Snaith, J. Lim, Toward Understanding Space-Charge Limited Current Measurements on Metal Halide Perovskites, ACS Energy Lett. 5 (2020) 376–384. https://doi.org/10.1021/acsenergylett.9b02720.
- [45] C. Liu, C. Igci, Y. Yang, O.A. Syzgantseva, M.A. Syzgantseva, K. Rakstys, H. Kanda, N. Shibayama, B. Ding, X. Zhang, V. Jankauskas, Y. Ding, S. Dai, P.J. Dyson, M.K. Nazeeruddin, Dopant-Free Hole Transport Materials Afford Efficient and Stable Inorganic Perovskite Solar Cells and Modules, Angew. Chemie Int. Ed. 60 (2021) 20489–20497. https://doi.org/10.1002/anie.202107774.